Oncogene (2011) 1–12

www.nature.com/onc

ORIGINAL ARTICLE

Control of tumor and microenvironment cross-talk by miR-15a and miR-16 in prostate cancer

M Musumeci[1,5], V Coppola[1,5], A Addario[1], M Patrizii[1], M Maugeri-Saccà[1], L Memeo[2], C Colarossi[2], F Francescangeli[1], M Biffoni[1], D Collura[3], A Giacobbe[3], L D'Urso[3], M Falchi[4], MA Venneri[1], G Muto[3], R De Maria[1,2,5] and D Bonci[1,5]

[1]*Department of Hematology, Oncology and Molecular Medicine, Istituto Superiore di Sanità, Rome, Italy;* [2]*Department of Experimental Oncology, Mediterranean Institute of Oncology, Catania, Italy;* [3]*Department of Urology, S. Giovanni Bosco Hospital, Turin, Italy and* [4]*AIDS National Center, Istituto Superiore di Sanità, Rome, Italy*

The interaction between cancer cells and microenvironment has a critical role in tumor development and progression. Although microRNAs regulate all the major biological mechanisms, their influence on tumor microenvironment is largely unexplored. Here, we investigate the role of microRNAs in the tumor-supportive capacity of stromal cells. We demonstrated that miR-15 and miR-16 are downregulated in fibroblasts surrounding the prostate tumors of the majority of 23 patients analyzed. Such downregulation of miR-15 and miR-16 in cancer-associated fibroblasts (CAFs) promoted tumor growth and progression through the reduced post-transcriptional repression of *Fgf-2* and its receptor *Fgfr1*, which act on both stromal and tumor cells to enhance cancer cell survival, proliferation and migration. Moreover, reconstitution of miR-15 and miR-16 impaired considerably the tumor-supportive capability of stromal cells *in vitro* and *in vivo*. Our data suggest a molecular circuitry in which miR-15 and miR-16 and their correlated targets cooperate to promote tumor expansion and invasiveness through the concurrent activity on stromal and cancer cells, thus providing further support to the development of therapies aimed at reconstituting miR-15 and miR-16 in advanced prostate cancer.
Oncogene advance online publication, 2 May 2011; doi:10.1038/onc.2011.140

Keywords: miRNA; microenvironment; cancer progression

Introduction

The prostate microenvironment is a variegate compartment in which the epithelial cells interact with mesenchymal and inflammatory cells in the presence of extracellular matrix (ECM) and soluble molecules (Bhowmick *et al*., 2004; De Marzo *et al*., 2007; Joyce and Pollard, 2009). The epithelial–stromal interaction has a fundamental role in organ formation and tissue homeostasis. However, during cancer development and progression, the tumor and its microenvironment co-evolve and contribute equally to the acquisition of the metastatic phenotype (Chung and Cunha, 1983; Cunha *et al*., 1983; Chung *et al*., 1989; Tuxhorn *et al*., 2002; Risbridger and Taylor, 2008; Thiery *et al*., 2009). In this context, the stroma acquires tumor-enhancing properties and is defined as 'reactive' (Tuxhorn *et al*., 2002; Josson *et al*., 2010). It has been suggested that a dysfunctional microenvironment can turn a prostatic hypertrophy into a prostate tumor through a process that involves vessel neo-formation and acquisition of androgen insensitivity (Chung *et al*., 1989; Wu *et al*., 1994; Hayward *et al*., 2001; Ao *et al*., 2007). Among the cell types cohabitating a reactive stroma, carcinoma-associated fibroblasts (CAFs) are thought to be the main actors, even though it is still unclear if these cells undergo irreversible alterations or epigenetic changes during tumor progression. A complex signaling and many growth factors connect stroma and cancer, including the vascular endothelial growth factor (VEGF-A), bone morphogenetic proteins (BMPs), insulin-like growth factors (IGFs), transforming growth factor-β (TGFβ), wingless-type ligand family (WNT), platelet-derived growth factor (PDGF) and fibroblast growth factors (FGFs) (van Moorselaar and Voest, 2002). In early tumor lesions, aberrant FGF-2 production and expression of its receptor (FGFR1) can alter the epithelial/stromal communication, which ensures the balance between growth and renewal of the epithelial compartment under physiological conditions (Kwabi-Addo *et al*., 2004). Moreover, FGF-2 production by both stromal and tumor cells promotes increased proliferation and metastasis formation in prostate cancer (PCa) (Cronauer *et al*., 1997; Giri *et al*., 1999; Yang *et al*., 2008). Thus, the FGF-2/FGFR axis is an attractive target for cancer therapy, in terms of both ligand sequestration and receptor inhibition (Smith *et al*., 2001; He *et al*., 2003). In the recent years, considerable attention has been devoted to the study of

Correspondence: Dr R De Maria or Dr D Bonci, Department of Hematology, Oncology and Molecular Medicine, Istituto Superiore di Sanità, Viale Regina Elena 299, Rome 00161, Italy.
E-mail: ruggero.demaria@iss.it or desiree.bonci@iss.it
[5]These authors contributed equally to this work.
Received 29 November 2010; revised 10 March 2011; accepted 21 March 2011

microRNAs (miRNAs), a family of small non-coding RNAs involved in the regulation of virtually all biological processes (Bartel, 2004; Calin and Croce, 2006). Many deregulated miRNAs contribute to tumor formation and therefore are potential therapeutic tools or targets against cancer cells. However, the influence of miRNAs on tumor microenvironment and CAFs is still largely unexplored. In a previous report, our group demonstrated that miR-15a (miR-15) and miR-16-1 (miR-16) reduction in tumor cells promotes prostate cancer progression, whereas their reconstitution impairs tumor growth (Bonci *et al*., 2008). Here, we extended our study to the prostate stromal compartment, demonstrating a fundamental role of miR-15 and miR-16 in tumor–stroma interaction. Our data offer new insights into the regulation of such cross-talk, thus providing considerable information for the development of innovative therapeutic approaches.

Results

miR-15 and miR-16 are downregulated in cancer-associated fibroblasts

During the setup of the *in situ* hybridization for clinical investigations, we noted that miR-15 and miR-16 (miR-15/16) downregulation in prostate cancer tissues was not confined to the tumor cell population. Therefore, we evaluated miR-15/16 levels in prostate stromal compartment through the analysis of 23 non-neoplastic and tumor tissues. A staining score was assigned using a semiquantitative evaluation: negative (score 0), weak (score 1), moderate (score 2) and strong staining (score 3). In the vast majority of tumor samples (17/23 for miR-15 and 18/23 for miR-16), fibroblasts were completely negative or displayed a weak staining (6/23 for miR-15 and 5/23 for miR-16). Non-neoplastic tissue-associated fibroblasts showed variable miRNA expression, ranging from negative (2/23 for miR-15 and 2/23 for miR-16) to weak (8/23 for miR-15 and 10/23 for miR-16), moderate (11/23 for miR-15 and 10/23 for miR-16) or strong staining (2/23 for miR-15 and 1/23 for miR-16). Overall, the majority of the stroma surrounding tumor samples analyzed showed an overt decrease in the levels of both miRNAs as compared with the stroma in the proximity of non-neoplastic gland (Figure 1a). The distribution of the scores among tumor and normal samples was significantly different as demonstrated by χ^2 test ($P<0.00001$ for miR-15 tumor vs normal stroma; $P<0.0001$ for miR-16 tumor vs normal stroma) (Figure 1b). Thus, there seems to be a considerable correlation between the low levels of miR-15 and miR-16 in the prostate stroma and the vicinity to the neoplastic tissue. In order to obtain a comparison between fibroblasts confining healthy and neoplastic gland from the same patient, we dissociated freshly collected tissue specimens from prostate cancer patients and isolated three couples of cancer and non-neoplastic associated fibroblast lines (CAFs and NAFs, respectively). We evaluated the purity of the cultures testing the expression of specific markers such as fibronectin, vimentin and CD90 by immunofluorescence or cytofluorimetric analysis (Figures 1c and d). As CAFs are usually recognized by the expression of α-smooth muscle actin (α-SMA) and closely resemble myofibroblasts residing in wound-healing sites, we analyzed them for α-SMA protein expression by western blotting (Figure 1e). Furthermore, we evaluated by real-time PCR miR-15 and miR-16 levels in the three populations of NAF/CAF, confirming a consistent reduction of miRNA expression in CAFs when compared with NAFs (Figure 1f). The clinical features of prostate cancer patients' specimens used for *in situ* hybridization and CAFs isolation are reported in Supplementary Table I.

miR-15 and miR-16 reconstitution impairs proliferation and supportive capability of cancer-associated fibroblasts

In order to evaluate the effect of miR-15 and miR-16 reconstitution on reactive stroma, CAFs were infected with the TWEEN (TW) lentiviral vector, engineered to express both *miR-15* and *miR-16* genes (miR-15/16) (Bonci *et al*., 2003, 2008). We infected CAFs at two different virus doses (1×10^6 and 5×10^5 TU/ml) and evaluated miRNA levels by real-time PCR (Supplementary Figure 1a). Cancer-associated fibroblasts transduced with the higher dose (1×10^6 TU/ml) of miR-15/16 viral supernatant dramatically decelerated their growth, undergoing progressive apoptosis extended in the majority of population 1 week after viral exposure (Figure 2a and Supplementary Figures 1b, d and e). On the other hand, CAFs transduced with lower miR-15/16 viral titer (5×10^5 TU/ml) decelerated slowly their growth (Figure 2b), showing modest cell death 3 weeks after infection (Supplementary Figure 1c). Empty vector (TW)-treated cells were used as control. Non-neoplastic fibroblasts infected at two different virus doses (1×10^6 and 5×10^5 TU/ml) did not show relevant toxicity (Supplementary Figure 1b and c) 3 weeks after infection. In order to test if the miR-15 and miR-16 effect can be reversed, we added miR-15/miR-16 antagomirs to fibroblast cultures transduced with empty or miRNA vectors (5×10^5 TU/ml) and evaluated cell proliferation after 3 days. We found that the specific antagomirs impair exogenous miRNA expression by real-time PCR and that miR15/16-transduced fibroblasts rescued their proliferation rate as compared with the control population (Supplementary Figures 1f and g). Thus, miR-15 and miR-16 reconstitution strongly impacts on CAF proliferation and viability in a dose-dependent manner, suggesting that miRNAs could be regulators of genes implicated in proliferation and survival, with possible implications in tumor–stroma cross-talk. In order to investigate the consequent effects of miRNA-reconstituted CAFs on tumor aggressiveness, we tested CAF-conditioned medium (CM) on different prostate cancer cell lines. We prepared a 24-h CM from cancer-associated fibroblasts transduced with empty or miR-15/16 vectors at 5×10^5 TU/ml and evaluated their ability to stimulate prostate cancer cell migration and proliferation. As CAFs are able to enhance the aggressiveness of tumor cells, a prostate tumor cell line

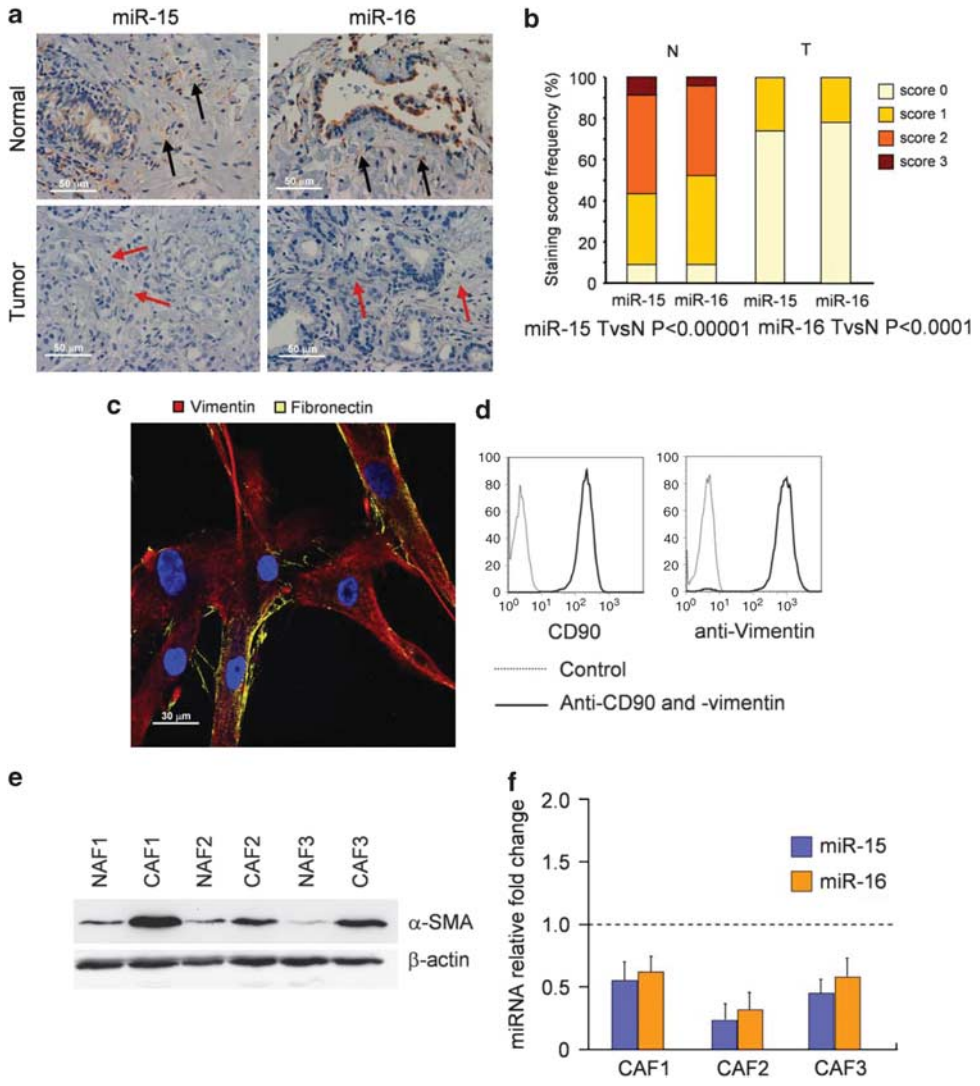

Figure 1 miR-15 and miR-16 expression in stroma compartment. miR-15 and miR-16 are downregulated in stroma surrounding neoplastic cells. (**a**) *In situ* hybridization analysis of miR-15 and miR-16 expression in stroma surrounding normal and tumor prostatic tissues (magnification ×40). Tumor (red arrows) and non-neoplastic prostate stroma cell areas (black arrows) are indicated. (**b**) Frequency distribution of 23 samples evaluated by *in situ* hybridization for miR-15 and miR-16 expression levels. A different color was assigned for each score (0–3). T, tumor microenvironment; N, non-neoplastic microenvironment. (**c**) Fibroblasts analyzed for vimentin and fibronectin expression by immunofluorescence. Blue color indicates DAPI nuclear staining. One image representative of different clones is reported. (**d**) FACS analysis of CD90 and vimentin expression on fibroblasts. (**e**) Western blotting of α-SMA protein in three CAF lines (CAF1–3) and compared with its normal counterpart (NAF1-3). β-Actin was used as internal control. (**f**) miR-15 and miR-16 expression levels evaluated by real-time PCR on CAFs and compared with NAFs derived from the same patient, indicated in the graph with the line at 1. Data were reported as mean ± s.d. of three independent experiments.

(RWPE-2) representative of early cancers was tested for its migratory capacity by Boyden chamber assay in the presence of TW or miR-15/16 CM. Non-conditioned culture medium was used as control. Whereas TW CM strongly enhanced the motility capacity of RWPE-2, miR-15/16 CM impaired the pro-migratory ability (Figure 2c). As AKT phosphorylation is associated with migration enhancement, in line with the observed effects, western blotting showed a reduction in AKT phosphorylation in cancer cells treated with miR-15/16 CM (Figure 2d). Another early prostate cancer cell line, CAHPV10, reduced its migratory capacity in miRNA CM as compared with TW CM (Supplementary Figure 2a). Likewise, metastatic PC3 cells reduced their motility capacity when maintained for 24 h in miR-15/16 CM, such as demonstrated by scratch-wound assay (Supplementary Figure 2b) (Kaminski *et al*., 2006). Moreover, the metastasis-derived prostate cancer cell line DU145 was maintained in culture with TW or miR-15/16 CM and analyzed after 24 h by bromodeoxyuridine incorporation assay. miR-15/16 CM treatment resulted in reduction of tumor cell proliferation, which correlated with a significant reduction in the percentage of cells in the S-phase of the cell cycle (Figure 2e) and with a parallel significant accumulation of cells in G0–G1-phase as shown by propidium iodide staining

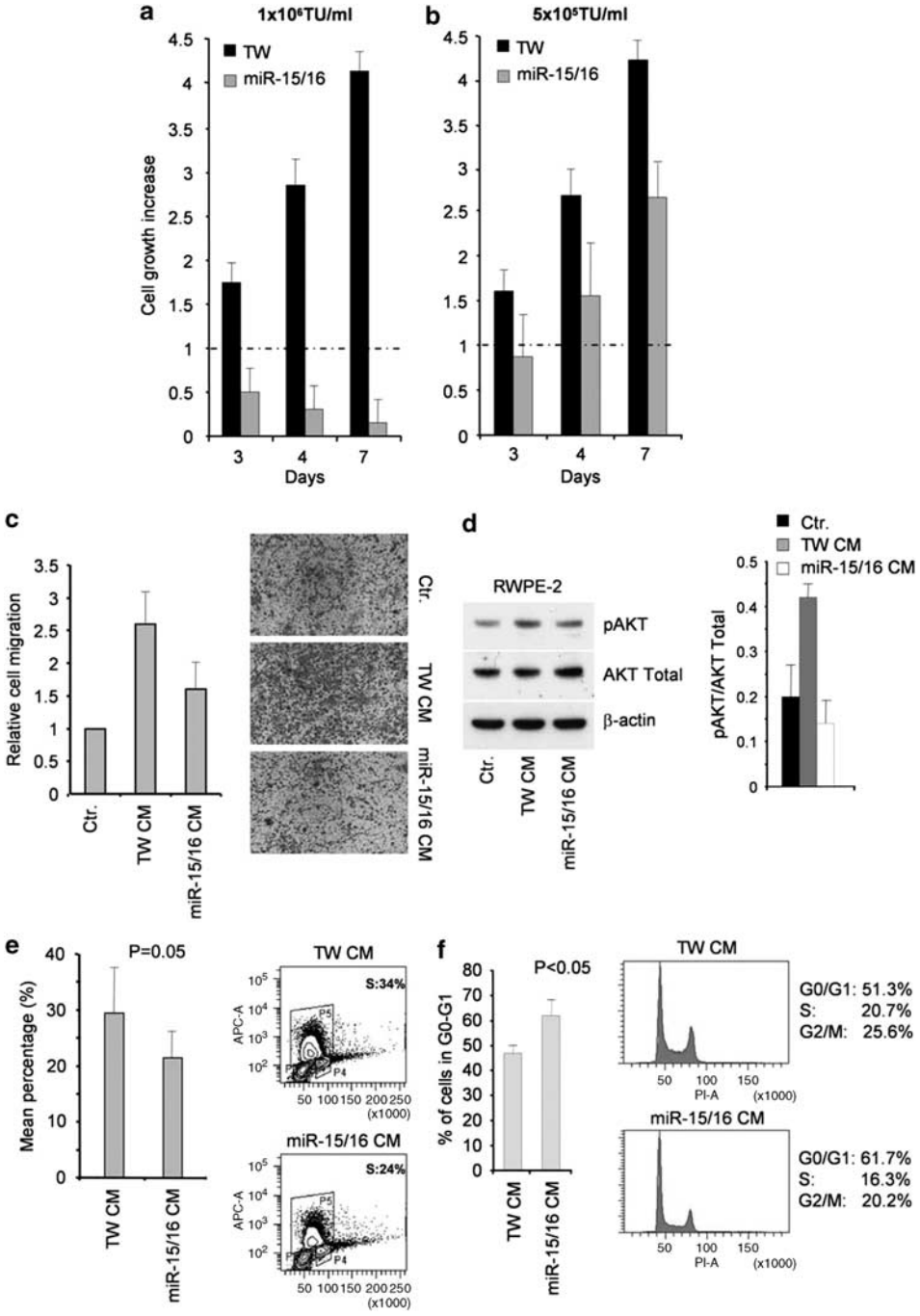

Figure 2 miR-15 and miR-16 reconstitution in fibroblasts. (**a**) Cell growth of CAFs infected with TW or miR-15/16 at a final viral dose of 1×10^6 TU/ml. (**b**) Cell growth of CAFs infected with TW or miR-15/16 at a final viral dose of 5×10^5 TU/ml. In (**a**) and (**b**) cell count has been performed by Trypan Blue staining and estimated over cell number at plating day. (**c**) Boyden chamber migration assay of early tumor RWPE-2 exposed for 48 h to the chemoattraction of CM collected from TW (TW CM) or miR-15/16 (miR-15/16 CM) transduced CAFs. Non-conditioned culture medium (Ctr), that is, cell culture medium, has been used as control. (**d**) Western blotting analysis of AKT phosphorylation compared with total AKT and endogenous control on RWPE-2 treated with CM collected from TW (TWCM) or miR-15/16 (miR-15/16 CM) transduced CAFs. Cells treated with non-conditioned medium were used as internal control (Ctr). One western blotting representative of CM collected from three CAF clones is reported. Histograms represent western blotting quantification of AKT phosphorylated protein and normalized over total AKT. β-Actin is additionally reported as endogenous control. In (**c**) and (**d**) non-conditioned culture medium has been used as control (Ctr). (**e**) Cell cycle analysis by cytofluorimetric profiling of BrdU/7AAD-stained metastatic cells, DU145, treated for 24 h with conditioned medium collected from TW (TW CM) or miR-15/16 (miR-15/16 CM) transduced CAFs. One experiment representative of three with different CAF clones is reported. Data are mean ± s.d. of three independent experiments. (**f**) Cytofluorimetric evaluation of propidium iodide (PI) staining in DU145 treated for 24 h with conditioned medium collected from TW (TW CM) or miR-15/16 (miR-15/16 CM) transduced CAFs. Results of BrdU assays and PI staining were analyzed by two-way ANOVA test.

(Figure 2f). Thus, re-expression of miR-15 and miR-16 in cancer-associated fibroblasts is able to reduce the stroma support capacity in terms of migration and proliferation of early and metastatic tumors, indicating that miR-15 and miR-16 reconstitution in CAFs interferes with the cross-talk between microenvironment and tumor, reducing cancer expansion capability.

FGF-2 and FGFR1 are new targets of miR-15 and miR-16
We subsequently investigated the existence of new miR-15 and miR-16 targets that could be responsible for the tumor-promoting activity of CAFs. We performed a bioinformatic analysis using TargetScan 4.2 and found that the FGF-2/FGFR1 axis was a likely candidate for this effect.

In particular, FGF-2-mediated activation of MEK/ERK signaling has a critical role in cancer cell proliferation, migration and invasiveness. In line with previous publications (Wernert *et al*., 2007; Sahni *et al*., 2008), we observed that FGF-2 treatment of prostate cancer cells DU145 and PC3 stimulates proliferation and migration, respectively, as shown by cell growth evaluation and scratch-wound assay (Supplementary Figures 2c and d). By luciferase assay, we demonstrated FGF-2 and FGFR1 as new direct targets of miR-15 and miR-16 (Supplementary Figure 2e). miR-15 and miR-16 reconstitution in cancer-associated fibroblasts confirmed FGF-2 and FGFR1 protein reduction, particularly of all the three FGF-2 isoforms (Figure 3a). FGF-2 treatment partially rescued the effect of miR-15/16 CM on DU145 cancer cell proliferation (Figure 3b). Among miR-15 and miR-16 published targets, *Ccnd1*, *Wnt3a* and *Bcl-2* genes promote prostate cell proliferation, invasion and survival. The analysis of WNT3A, CCND1 and BCL-2 expression by western blotting in TW and miR-15/16 transduced fibroblasts confirmed that the products of these genes are miR-15 and miR-16 targets also in the stromal compartment, underlying the multiple synergic activity of the miRNAs on cancer progression (Figure 3c). Although we cannot exclude the involvement of additional unknown targets, it is likely that miR-15/16-mediated reduction of fibroblast supportive capacity can be caused by targeting the FGF-2/FGFR1 axis, WNT3A, CCND1 and BCL-2. Furthermore, western blot analysis showed a reduction of p-AKT and p-ERK in miR-15/16-transduced fibroblasts, as a likely consequence of FGF-2/FGFR1 and WNT3A downregulation (Figure 3c). Likewise, DU145 treated with miR-15/16 fibroblast CM (miR-15/16 viruses were used at a final concentration of 5×10^5 TU/ml) showed the same decrease in signaling activation (Supplementary Figure 2f).

miR-15 and miR-16 block stromal tumor support in vivo
Microenvironment aberrant stimuli can transform non-neoplastic prostate epithelium cells into cancer cells (Hayward *et al*., 2001; Ao *et al*., 2007). Moreover, the cancer–stroma interaction can enhance survival and tumor spreading, leading to metastasis formation (Thiery, 2002; Kalluri and Weinberg, 2009; Polyak and Weinberg, 2009). We explored the pro-tumorigenic effects of the cancer-associated stroma *in vivo* by inoculating a tumor cell line representative of early tumors (RWPE-2) into a permissive site such as the renal capsule of NOD-SCID mice. RWPE-2 cells were infected with a lentiviral vector (TW-Luc) containing the luciferase gene for *in vivo* imaging. We co-injected RWPE-2 with TW or miR-15/16 transduced fibroblasts (empty or miR-15/16 vectors were used at a final concentration of 5×10^5 TU/ml). Three weeks after injection, we evaluated tumor expansion by *in vivo* imaging (IVIS system). Empty vector-treated fibroblasts strongly promoted tumor growth by about fourfold as compared with miR-15/16 transduced fibroblasts (Figure 4a). We therefore sacrificed the mice and analyzed by histology tumor morphology and vascularization. Hematoxylin and eosin (H&E) staining and anti-CD31 immunofluorescence analysis revealed that while co-injection with TW fibroblasts promoted the invasion of RWPE-2 cells into the renal parenchyma coupled with new vessel formation, the co-injection with miR-15/16-transduced fibroblasts was ineffective (Figures 4a and b). We next analyzed the effect of miR-15/16 reconstitution on a metastasis-derived prostate cancer model. DU145 tumor cells were injected subcutaneously together with TW- or miR-15/16-transduced fibroblasts (1×10^5 fibroblasts and 2×10^5 DU145) obtained with a virus concentration that did not dramatically affect cell survival within the first 3 weeks (5×10^5 TU/ml). As observed for RWPE-2 cells, miR-15/16-transduced fibroblasts severely impaired the tumor growth generated by DU145 cells co-inoculated with TW-treated fibroblasts (Figure 4c). H&E staining showed that the cancer cells mixed with TW fibroblasts functionally recruit and interact with stroma, creating a large front of invasion, whereas miR-15/16-transduced fibroblasts significantly impaired prostate cancer communication, producing a more homogeneous and compact tumor mass (Figure 4d). Moreover, we observed a considerable reduction of FGF-2 both in the stroma and in the cancer compartment in tumor masses co-injected with miR-15/16-transduced CAFs (Figure 5a). In addition, at higher magnification we observed some degree of alteration of presumable lymphatic or blood vessels (Figure 5a). As FGF signaling also promotes tumor angiogenesis, we extended our study to the evaluation of neovasculature formation in these subcutaneous tumor xenografts. Immunofluorescence analysis on cancer masses demonstrated a strong reduction of CD31+ vessels at the periphery and inside the inner mass of tumor xenografts obtained with miR15/16-transduced fibroblasts (Figures 5b and c), suggesting that the reconstitution of miR-15/16 impaired the production of angiogenic factors. To mimic the formation of micro-foci lesions, where the stromal population is more abundant than the tumor compartment, we co-injected DU145 and cancer fibroblast cells in NOD-SCID mice at a final ratio of 1:2 (1×10^5 DU145 and 2×10^5 fibroblasts). Cancer cells co-inoculated with a higher amount of miR-15/16 fibroblasts were unable to form tumors, whereas empty vector fibroblasts mixed with tumor cells strongly

promoted cancer formation (Figure 5d), further indicating that transduction of miR-15/16 in cancer-associated fibroblasts is able to disrupt microenvironment–tumor cross-talk. As we previously demonstrated that loss of miR-15/16 expression in prostate cancer cells significantly contributes to tumor progression and that their reconstitution caused tumor regression *in vitro* and *in vivo*, the proposed study offers a potential dual therapeutic approach by simultaneously blocking tumor and its supportive microenvironment.

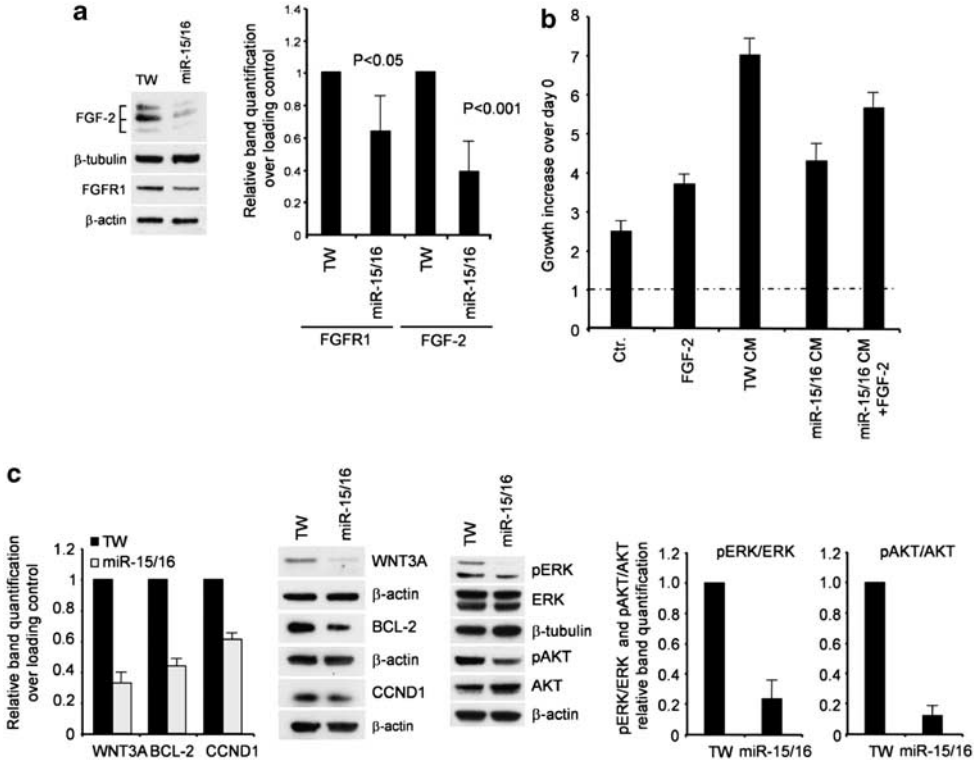

Figure 3 Effect of miR-15 and miR-16 on the cancer support capacity of fibroblasts. (**a**) Western blotting analysis of FGF-2 and FGFR1 tested in CAFs transduced with TW or miR-15/16. β-Tubulin and β-actin were used as reference controls. TW or miR-15/16 viruses were used at a final concentration of 5×10^5 TU/ml. One representative of the three clones is reported. The histograms report the FGF-2 and FGFR1 proteins mean reduction normalized over endogenous control and reported as decrease over TW samples. (**b**) Cell growth estimation of DU145 cells maintained in culture for 24 h with conditioned medium collected from TW (TW CM) or miR-15/16-transduced CAFs (miR-15/16 CM) or miR-15/16-transduced CAFs with 10 ng/ml of FGF-2 (miR-15/16 CM + FGF-2). Non-conditioned culture medium with (10 ng/ml) or without FGF-2 has been used as control (Ctr; FGF-2, 10 ng/ml). Data are mean ± s.d. of three independent experiments. (**c**) To the left, western blotting analysis of WNT3A, CCND1 and BCL-2 in CAFs transduced with TW or miR-15/16. The histograms report the western blotting bands quantification normalized over endogenous control and estimated over TW sample. To the right, signaling transduction evaluation by western blotting of pAKT and pERK in CAFs transduced with TW and miR-15/16; total AKT, ERK, β-tubulin and β-actin were reported as controls. One western blotting representative of three CAF clones is shown. The histograms report the western blotting bands quantification for pERK and pAKT normalized over total ERK and AKT proteins, respectively, and estimated as decrease over TW sample.

Figure 4 miR-15 and miR-16 modulate early and aggressive tumor growth *in vivo*. RWPE-2 cells (2×10^5) transduced with viral particles containing luciferase gene were injected into the subrenal capsule space (SRC) of NOD-SCID mice, mixed with TW (TW) or miR-15/16 (miR-15/16) transduced CAFs (1×10^5). (**a**) Monitoring of tumor growth 3 weeks after injection by IVIS imaging system. H&E staining of relative masses. One representative image for each group of mice is reported. The histograms show tumor mass expansion when injected into renal capsule and evaluated in three mice for each group in two independent experiments. The tumor area percentage was calculated as fold change over tissue total area. The red arrows mark tumor (T) front of invasion. Phosphate-buffered saline was injected alone into the renal capsule space for surgery control. In order to better visualize and anatomically indicate the renal capsule membrane and space, the yellow line and black arrows were used both in phosphate-buffered saline (PBS) and fibroblast/tumor mixed-population images. (**b**) Mouse CD31 endothelial cell marker staining on tumor masses produced in (**a**). Merge represents the CD31 (red) and DAPI staining (blue). (**c**) Size of subcutaneous xenografts obtained after injection of 2×10^5 DU145 cells alone (DU145) or in combination with 1×10^5 CAFs transduced with control (TW) or miR-15/16 vectors (miR-15/16). CAFs were used as control. The graph reports the mean of four mice for each group and for three different CAF clones in two independent experiments. (**d**) H&E staining of subcutaneously grown tumors as in (**c**) and explanted 4 weeks after injection. T, DU145 cells; S, human cancer-associated stroma. Yellow arrows indicate fibroblasts interacting with tumor mass. One and two images representative of periphery and inner tumor mass, respectively, are reported.

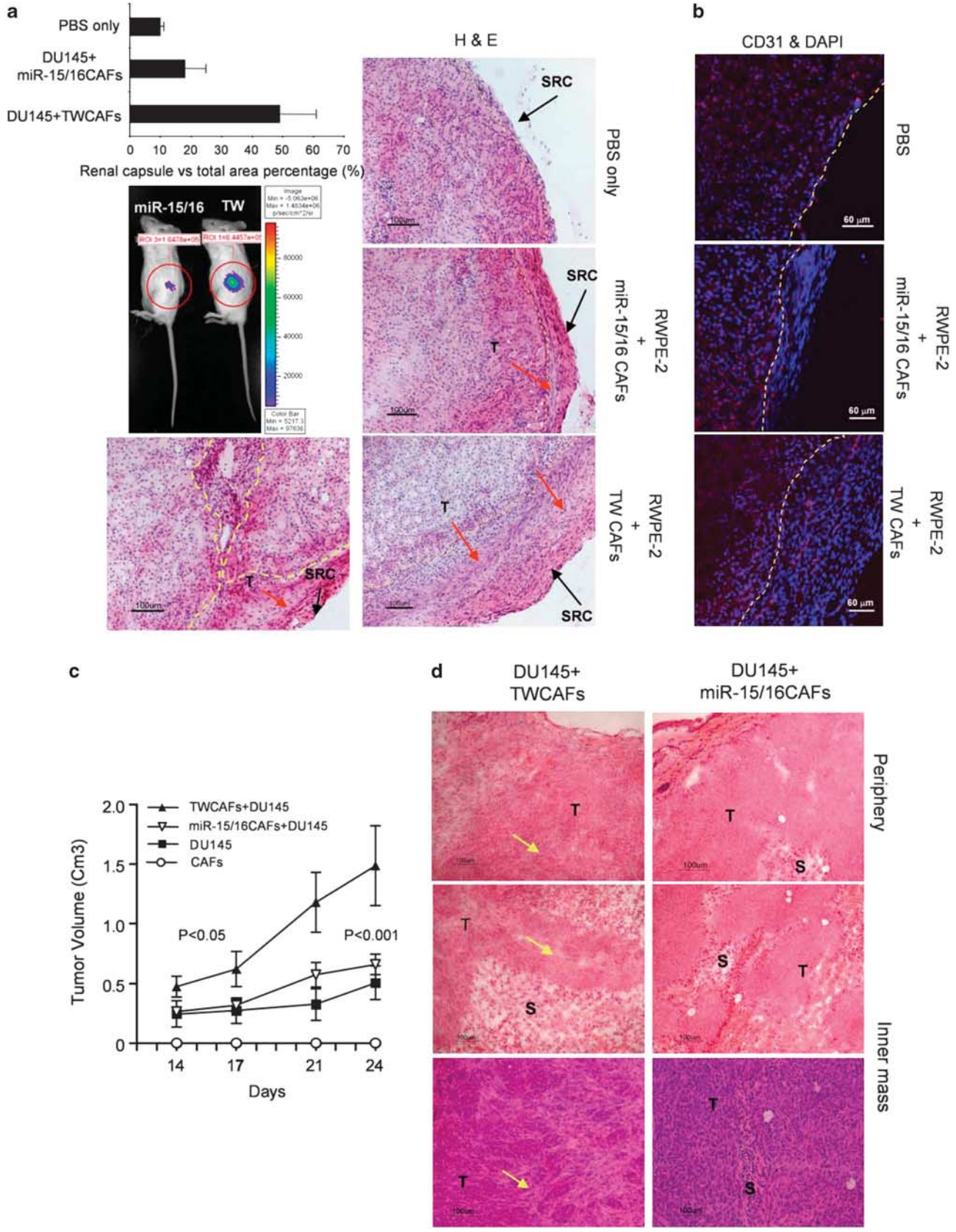
a
PBS only
DU145+ miR-15/16CAFs
DU145+TWCAFs
0 10 20 30 40 50 60 70
Renal capsule vs total area percentage (%)
miR-15/16
TW
H & E
SRC
T
PBS only
RWPE-2 + miR-15/16 CAFs
RWPE-2 + TW CAFs
b
CD31 & DAPI
PBS
RWPE-2 + miR-15/16 CAFs
RWPE-2 + TW CAFs
60 µm
c
TWCAFs+DU145
miR-15/16CAFs+DU145
DU145
CAFs
Tumor Volume (Cm3)
2.0
1.5
1.0
0.5
0
P<0.05
P<0.001
14 17 21 24
Days
d
DU145+ TWCAFs
DU145+ miR-15/16CAFs
Periphery
Inner mass
T
S

Discussion

Prostate cancer cells recruit a functional supportive stroma to create a favorable microenvironment that promotes cancer growth and spreading at primary and metastatic sites (Thiery, 2002; Kalluri and Weinberg, 2009; Polyak and Weinberg, 2009). Recent observations indicate that prostate tumor microenvironment is directly implicated in the resistance to therapy (Efstathiou and Logothetis, 2010). However, the complex interactions between stroma and neoplastic cells are largely unexplored. Here, we demonstrated that miR-15 and miR-16 are often downmodulated in the tumor-surrounding stroma, as a possible result of a conditioning of microenvironment by cancer cells.

As loss of miR-15 and miR-16 has been described as a key event in cancer progression in different tumor types (Cimmino *et al*., 2005; Bandi *et al*., 2009; Bhattacharya *et al*., 2009; Roccaro *et al*., 2009; Klein *et al*., 2010), our data suggest that the tumor suppressor activity of miR-15 and miR-16 is not confined to the cancer cell compartment, but is shared by the tumor microenvironment. MicroRNAs control the expression of multiple targets, offering a great advantage as a possible multi-blocking therapeutic approach. miR-15 and miR-16 can target several oncogenes, such as *Bcl-2*, *Ccnd1, Ccne1*, *Bmi-1* and *Wnt* family members, which promote cell proliferation, survival and invasion. Moreover, recent data suggest that miR-15 and miR-16 control the expression of VEGF and IL-6, which are able to promote tumor angiogenesis and metastatic homing to the bones, respectively (Iliopoulos *et al*., 2009; Karaa *et al*., 2009; Roccaro *et al*., 2009). The tumor microenvironment cross-talk is mediated by many growth factors, including FGF-2. In PCa, stromal FGF-2 level increases in parallel with the acquisition of aggressive properties. Whereas FGF-2 production in early tumors is confined to stromal cells, in advanced prostate cancer FGF-2 is overproduced by tumor cells (Giri *et al*., 1999; Kwabi-Addo *et al*., 2004). Of note, in prostate cancer cell lines, the levels of FGF-2 and FGFR1 have been shown to increase proportionally to the degree of cancer aggressiveness and castration resistance (Nakamoto *et al*., 1992; Cronauer *et al*., 1997). The analysis of tumor specimens has shown that enhanced FGF signaling results in increased proliferation, invasiveness and resistance to therapy in several solid and hematological malignancies (Menzel *et al*., 1996; Konig *et al*., 1997; Song *et al*., 2000; Sezer *et al*., 2001; Acevedo *et al*., 2009; Turner *et al*., 2010). Moreover, hemi- or homozygous inactivation of *Fgf-2* alleles in TRAMP mice with transgenic prostate adenocarcinoma resulted in increased survival by inhibiting progression toward a poorly differentiated and highly metastatic phenotype (Polnaszek *et al*., 2003). In our study, we showed that *Fgf-2* and *Fgfr1* are new targets for miR-15 and miR-16, thus providing further information on the molecular mechanisms through which tumor and stroma influence each other and promote tumor growth and progression. Reconstitution of miR-15 and miR-16 in CAFs severely impaired tumor-supporting capacity, as shown by reduction of proliferation and migration *in vitro* and impaired tumor expansion *in vivo*. The FGF-2/FGFR1 axis promotes tumor angiogenesis, triggering the generation of aberrant vessels, which, in turn, may impair drug delivery (Winter *et al*., 2007). Our data report a considerable reduction in neo-angiogenesis upon injection in immunocompromised mice of tumor cells mixed with CAFs transduced with miR-15 and miR-16, suggesting a role of their angiogenic targets in this process.

Different approaches have been attempted to inhibit FGFR-mediated signaling, such as developing antibodies to target receptors (He *et al*., 2003) or small-molecule inhibitors blocking the catalytic kinase domain (Mohammadi *et al*., 1997). Compounds that inhibit FGF signaling, such as suramin, have been found to be able to enhance the antitumor effect of doxorubicin on PCa (Zhang *et al*., 2001). The relevance of the FGF-2/FGFR axis is further corroborated by some phase II studies of BIBF 1120, an orally triple angiokinase (VEGFR, PDGFR, FGFR) inhibitor, which laid the basis for two phase III trials that are currently undergoing in advanced/metastatic lung cancer patients. Our results indicate an innovative molecular tool to inhibit FGF-2/FGFR1 signaling and, more importantly, propose a strategy to obtain a therapeutic targeting of both tumor and stroma compartments. Although the targets of miRNAs may vary depending on the cell type of tissue where they are expressed, we confirmed in CAFs

Figure 5 Effect on angiogenesis of miR-15 and miR-16 reconstitution in CAFs. (**a**) FGF-2 expression evaluated by immunohistochemistry on tumor masses obtained by subcutaneous injection of DU145 cells mixed with TW or miR-15/16-transduced CAFs. The percentage decrease of FGF-2-positive cells in the miRNA fibroblasts/tumors (range between minimal and maximal values) was calculated as fold change over TW fibroblasts/tumor-positive cells. Each of these values was derived from the counting of at least three high-power microscopic fields per slide per inoculated mouse. Tumors were explanted 4 weeks after injection. An IgG antibody was used as negative control (Control). Red arrows indicate hypothetical vessels (upper panels $\times 10$ magnification, bottom panels $\times 40$). (**b**) Mouse CD31 antigen immunofluorescence staining (Red) on tumors reported in (**a**). Blue color represents DAPI nuclear staining. (**c**) Neo-angiogenesis evaluation as reported in (**b**) and estimated as decrease fold change of the percentage of CD31-positive cells both in periphery and in inner mass, in the miRNA fibroblasts/tumors (range between minimal and maximal values) over TW fibroblasts/tumor-positive cells. The periphery and inner masses of the xenograft lesions showed a consistent reduction of the percentage of neo-formed vessels in miRNA fibro/tumor-injected mice as reported in the histograms. The percentage of positive cells was calculated over total area. Each of these values was derived from the counting of at least two high-power microscopic fields per inoculated mouse. For experiments reported in (**a–c**) three mice per group for three clones were analyzed. (**d**) Size of subcutaneous xenografts obtained after injection of 1×10^5 DU145 cells alone (DU145) or in combination with 2×10^5 CAFs transduced with control (TW) or miR-15/16 vectors. Four mice for each group and for two different CAF clones were used in two independent experiments. (**e**) Representative scheme of the molecular cross-talk driven by miR-15 and miR-16 deficiency, recapitulating the data presented in the study (continuous line) or reported in published articles (dotted lines).

that *Ccnd1, Wnt3A* and *Bcl-2* are targets of miR-15 and miR-16, demonstrating the multi-targeting and tumor-suppressor activity of these miRNAs and their role in tumor etiology, while providing new insights into the stromal signaling pathways. While a few reports show that miR-15 and miR-16 can be unregulated in cancer

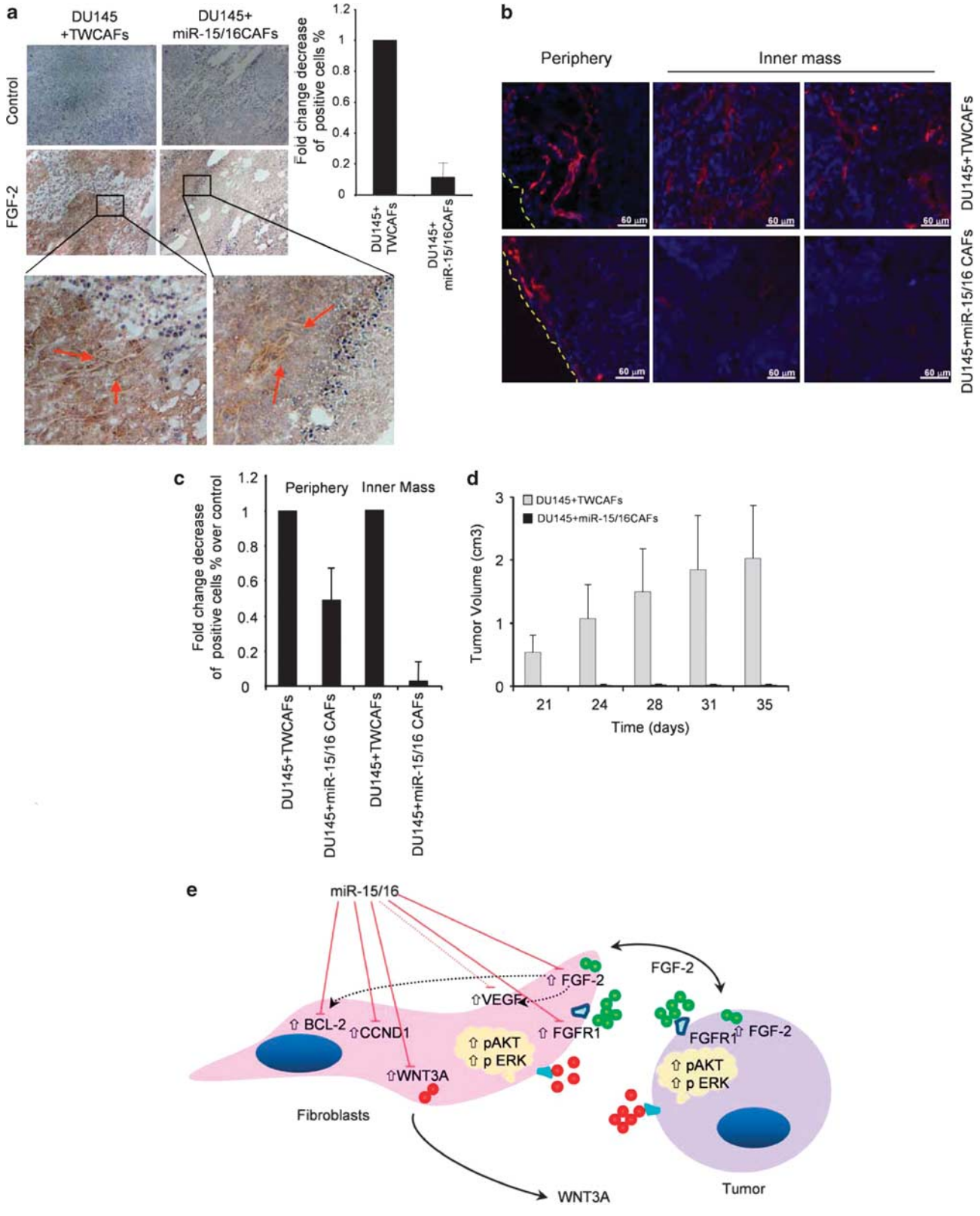

(Shin *et al*., 2011; Navarro *et al*., 2011), a number of articles show that miR-15 and miR-16 act as tumor controller (Aqeilan *et al*., 2010). However, our data suggest, as proposed in Figure 5e, that miR-15 and miR-16 may be involved in a molecular loop in which the tumor and microenvironment co-evolve, underlining the importance of miRNA in microenvironment homeostasis and providing a proof-of-concept for innovative therapeutic applications directed against not only the cancer cells but also the tumor microenvironment.

As it is extremely difficult to hypothesize a therapeutic approach with agents targeting exclusively malignant stroma but not tumor cells, miR-15 and miR-16 reconstitution appears as an innovative approach to develop new therapeutics co-targeting simultaneously cancer and its microenvironment. In conclusion, we demonstrated that miR-15 and miR-16 act as tumor suppressors both on tumor and on stromal cells. As miR-15 and miR-16 deregulation are involved in several tumors, the ability to target the microenvironment may enhance their therapeutic efficacy in different malignancies.

Materials and methods

Fibroblast isolation and CM preparation

Fibroblasts were isolated after mechanical and enzymatic dissociation of prostate surgical specimens with 150 μg/ml collagenase II (Gibco, Invitrogen, Carlsbad, CA, USA). The homogenate suspension was put in culture in plates with Dulbecco's modified Eagle's medium (Gibco, Invitrogen) supplemented with 10% fetal bovine serum (FBS), 2 mM glutamine, 100 U/ml penicillin and 100 μg/ml streptomycin. Fibroblast separation from epithelial cells was obtained by treatment with diluted (1 g/l) trypsin solution for 1–2 min once or twice. This procedure is based on a higher sensitivity of fibroblasts to trypsin. All fibroblast experiments were performed over 2 to 3 weeks after isolation. The frequency of culture isolation is 90% for CAFs and 10% for NAFs. Tissues were obtained from radical prostatectomy at the Department of Urology, S. Giovanni Bosco Hospital of Turin, Italy. Benign and neoplastic tissue specimens were taken from the prostate base in the transition zone and the suspicious areas in the peripheral zone, respectively. The tumoral or non-tumoral nature of each sample was confirmed by histopathological examination. All samples were collected with the informed consent of the patients and clinical features are reported in Supplementary Table I.

CM was prepared by cultivating human prostate cancer fibroblasts infected with TW or miR-15/16 at 5×10^5 TU/ml in RPMI supplemented with 0.5% FBS or in keratinocyte serum-free medium for 24 h; CM was then collected, filtered with 0.22 μm filters and kept at −20 °C until use. CMs were prepared after 48 h from virus infection. For CM preparation fibroblasts after viral exposure were extensively washed with phosphate-buffered saline and cultivation medium was tested on a highly infectable cell line, Hela, and analyzed for EGFP expression to exclude viral particle residues. In all experiments CM was then diluted 1:2 with fresh medium. The control medium was RPMI 0.5% FBS or keratinocyte serum-free medium. To examine the effects of fibroblast CM on cancer cell proliferation, DU145 cells were incubated for 24 h with CM from CAFs infected with TW or miR-15/16. Cells cultivated in RPMI medium with 0.5% FBS were used as control. Cell growth was evaluated by Trypan Blue staining.

Target screening. In this study, we used a publicly available search engine for target prediction: TargetScan, http://genes.mit.edu/targetscan (Lewis *et al*., 2003, 2005; Bartel, 2004).

In situ *hybridization, immunohistochemistry*

Locked nucleic acid-modified probes biotinylated at the 5′ end (Exiqon, Vedbaek, Denmark) were used to detect the *in situ* hybridization signal for miR-15 and miR-16 on formalin-fixed, paraffin-embedded prostate tissues. *In situ* hybridization was performed as previously described in Bonci *et al*. (2008) and analysis of staining score in stroma surrounding neoplastic and non-neoplastic prostate epithelium was performed by an experienced pathologist. For analysis of *in vivo* experiments, tumor masses, both obtained from mice injected subcutaneously and into subrenal capsule, were snap-frozen in OCT and stored at −80 °C. Cryostatic sections were stained with hematoxylin and eosin, dehydrated and mounted with xylene. For FGF-2 immunohistochemistry detection, frozen sections (3–5 μm), obtained using a cryomicrotome (Kriostat 1720 MGW Leitz, Melville, NY, USA), were fixed in paraformaldehyde 4% at room temperature for 15 min; endogenous peroxidase activities were blocked using 0.03% hydrogen peroxide for 15 min; sections were incubated at 4 °C overnight with anti-FGF-2 (1:100; 610072; BD Pharmingen, San Jose, CA, USA). Sections were then processed using avidin–biotin–peroxidase complex (ULTRATEK HRP SCY tek UCS Diagnostic s.r.l., Morlupo, RM, Italy), counterstained with hematoxylin and permanently mounted under a coverslip with DPX (Sigma, St Louis, MO, USA).

For CD31 immunofluorescence analysis, cryostatic sections were fixed with paraformaldehyde and then blocked with 5% serum in phosphate-buffered saline containing 1% bovine serum albumin and 0.1% Triton X-100. After 1 h of incubation at room temperature, sections were stained overnight at 4 °C with phycoerythrin mouse anti-CD31 (1:50; 553373; BD Pharmingen). Cell nuclei were stained using 4′,6-diamidino-2-phenylindole. Fluorescent signals from a single optical section were acquired by a three-laser confocal microscope (Olympus FV1000, Segrate, MI, Italy).

In vivo *models*

Six- to eight-week-old male NOD-SCID mice were purchased from Charles River Laboratories (Calco, LC, Italy) and housed in groups of four in isolated ventilated cages; food and water were provided *ad libitum*. All animal procedures were performed according to the protocol approved by the Istituto Superiore di Sanità Animal Care Committee. A total of 100 μl of cell suspension in matrigel (1:1, vol/vol) was subcutaneously injected into the flank of mice. CAFs were irradiated with 10 cGy using a cesium source before *in vivo* inoculation. For the subrenal capsule (SRC) injection animals were anesthetized with a mixture of ketamine (100 mg/kg) and xylazine (10 mg/kg). Under sterile conditions, a skin incision of approximately 1 cm was made along the dorsal midline of an anesthetized mouse. With the mouse lying on its side, a body wall incision was then made slightly shorter than the long axis of the kidney. The left kidney was slipped out of the body by applying pressure on both sides of the organ using the forelimb and thumb. Injection of a mixture of cells resuspended in 15 μl of matrigel was administered with a 29-G needle in the subcapsular space of the kidney, taking care not to damage the parenchyma. Phosphate-buffered saline was injected as surgery control. The kidney was then gently eased back into the peritoneal space; the body wall incision was closed using a 4/0 absorbable suture, while the skin incision was closed with surgical staples. Approximately 1 ml of saline solution was

administered subcutaneously immediately after surgery. For *in vivo* imaging analysis, mice were injected intraperitoneally with 150 mg/kg D-luciferin (Caliper Life Sciences, Tremblay en France, France) 10 min before imaging and then were sedated with 20 mg/kg valium. A cryogenically cooled imaging system (IVIS 100 Imaging System, Xenogen, Tremblay en France, France) was used for data acquisition. Whole animal imaging was used to monitor tumor growth; signal intensities were quantified as the sum of all detected photons.

Statistical analysis. Data are presented as the mean + s.d. Results of bromodeoxyuridine, luciferase assays, propidium iodide staining and *in vivo* experiments were analyzed by two-way analysis of variance test. *In situ* hybridization data were analyzed with χ^2-test. The immunofluorescence and immunohistochemistry figures were quantified by the KS300 (Carl Zeiss, Jena, Germany) image analysis software and expressed as the percentage of positive area over the total tissue area.

For additional information and methods see Supplementary files.

Conflict of interest

The authors declare no conflict of interest.

Acknowledgements

We thank Giuseppe Loreto and Maria Rita Pulvirenti for technical assistance. This work was supported by the Italian Health Ministry with 'Under forty researchers 2007'and Italy-USA programs and by the Italian Association for Cancer Research (AIRC).

References

Acevedo VD, Ittmann M, Spencer DM. (2009). Paths of FGFR-driven tumorigenesis. *Cell Cycle* **8**: 580–588.

Ao M, Franco OE, Park D, Raman D, Williams K, Hayward SW *et al*. (2007). Cross-talk between paracrine-acting cytokine and chemokine pathways promotes malignancy in benign human prostatic epithelium. *Cancer Res* **67**: 4244–4253.

Aqeilan RI, Calin GA, Croce CM. (2010). miR-15a and miR-16-1 in cancer: discovery, function and future perspectives. *Cell Death Differ* **17**: 215–220.

Bandi N, Zbinden S, Gugger M, Arnold M, Kocher V, Hasan L *et al*. (2009). miR-15a and miR-16 are implicated in cell cycle regulation in a Rb-dependent manner and are frequently deleted or down-regulated in non-small cell lung cancer. *Cancer Res* **69**: 5553–5559.

Bartel DP. (2004). MicroRNAs: genomics, biogenesis, mechanism, and function. *Cell* **116**: 281–297.

Bhattacharya R, Nicoloso M, Arvizo R, Wang E, Cortez A, Rossi S *et al*. (2009). MiR-15a and MiR-16 control Bmi-1 expression in ovarian cancer. *Cancer Res* **69**: 9090–9095.

Bhowmick NA, Neilson EG, Moses HL. (2004). Stromal fibroblasts in cancer initiation and progression. *Nature* **432**: 332–337.

Bonci D, Cittadini A, Latronico MV, Borello U, Aycock JK, Drusco A *et al*. (2003). Advanced' generation lentiviruses as efficient vectors for cardiomyocyte gene transduction *in vitro* and *in vivo*. *Gene Ther* **10**: 630–636.

Bonci D, Coppola V, Musumeci M, Addario A, Giuffrida R, Memeo L *et al*. (2008). The miR-15a-miR-16-1 cluster controls prostate cancer by targeting multiple oncogenic activities. *Nat Med* **14**: 1271–1277.

Calin GA, Croce CM. (2006). MicroRNA-cancer connection: the beginning of a new tale. *Cancer Res* **66**: 7390–7394.

Chung LW, Chang SM, Bell C, Zhau HE, Ro JY, von Eschenbach AC. (1989). Co-inoculation of tumorigenic rat prostate mesenchymal cells with non-tumorigenic epithelial cells results in the development of carcinosarcoma in syngeneic and athymic animals. *Int J Cancer* **43**: 1179–1187.

Chung LW, Cunha GR. (1983). Stromal-epithelial interactions: II. Regulation of prostatic growth by embryonic urogenital sinus mesenchyme. *Prostate* **4**: 503–511.

Cimmino A, Calin GA, Fabbri M, Iorio MV, Ferracin M, Shimizu M *et al*. (2005). miR-15 and miR-16 induce apoptosis by targeting BCL2. *Proc Natl Acad Sci USA* **102**: 13944–13949.

Cronauer MV, Hittmair A, Eder IE, Hobisch A, Culig Z, Ramoner R *et al*. (1997). Basic fibroblast growth factor levels in cancer cells and in sera of patients suffering from proliferative disorders of the prostate. *Prostate* **31**: 223–233.

Cunha GR, Chung LW, Shannon JM, Taguchi O, Fujii H. (1983). Hormone-induced morphogenesis and growth: role of mesenchymal-epithelial interactions. *Recent Prog Horm Res* **39**: 559–598.

De Marzo AM, Platz EA, Sutcliffe S, Xu J, Gronberg H, Drake CG *et al*. (2007). Inflammation in prostate carcinogenesis. *Nat Rev Cancer* **7**: 256–269.

Efstathiou E, Logothetis CJ. (2010). A new therapy paradigm for prostate cancer founded on clinical observations. *Clin Cancer Res* **16**: 1100–1107.

Giri D, Ropiquet F, Ittmann M. (1999). Alterations in expression of basic fibroblast growth factor (FGF) 2 and its receptor FGFR-1 in human prostate cancer. *Clin Cancer Res* **5**: 1063–1071.

Hayward SW, Wang Y, Cao M, Hom YK, Zhang B, Grossfeld GD *et al*. (2001). Malignant transformation in a nontumorigenic human prostatic epithelial cell line. *Cancer Res* **61**: 8135–8142.

He QM, Wei YQ, Tian L, Zhao X, Su JM, Yang L *et al*. (2003). Inhibition of tumor growth with a vaccine based on xenogeneic homologous fibroblast growth factor receptor-1 in mice. *J Biol Chem* **278**: 21831–21836.

Iliopoulos D, Hirsch HA, Struhl K. (2009). An epigenetic switch involving NF-kappaB, Lin28, Let-7 MicroRNA, and IL6 links inflammation to cell transformation. *Cell* **139**: 693–706.

Josson S, Matsuoka Y, Chung LW, Zhau HE, Wang R. (2010). Tumor-stroma co-evolution in prostate cancer progression and metastasis. *Semin Cell Dev Biol* **21**: 26–32.

Joyce JA, Pollard JW. (2009). Microenvironmental regulation of metastasis. *Nat Rev Cancer* **9**: 239–252.

Kalluri R, Weinberg RA. (2009). The basics of epithelial-mesenchymal transition. *J Clin Invest* **119**: 1420–1428.

Kaminski A, Hahne JC, Haddouti el M, Florin A, Wellmann A, Wernert N. (2006). Tumour-stroma interactions between metastatic prostate cancer cells and fibroblasts. *Int J Mol Med* **18**: 941–950.

Karaa ZS, Iacovoni JS, Bastide A, Lacazette E, Touriol C, Prats H. (2009). The VEGF IRESes are differentially susceptible to translation inhibition by miR-16. *RNA* **15**: 249–254.

Klein U, Lia M, Crespo M, Siegel R, Shen Q, Mo T *et al*. (2010). The DLEU2/miR-15a/16-1 cluster controls B cell proliferation and its deletion leads to chronic lymphocytic leukemia. *Cancer Cell* **17**: 28–40.

Konig A, Menzel T, Lynen S, Wrazel L, Rosen A, Al-Katib A *et al*. (1997). Basic fibroblast growth factor (bFGF) upregulates the expression of bcl-2 in B cell chronic lymphocytic leukemia cell lines resulting in delaying apoptosis. *Leukemia* **11**: 258–265.

Kwabi-Addo B, Ozen M, Ittmann M. (2004). The role of fibroblast growth factors and their receptors in prostate cancer. *Endocr Relat Cancer* **11**: 709–724.

Lewis BP, Burge CB, Bartel DP. (2005). Conserved seed pairing, often flanked by adenosines, indicates that thousands of human genes are microRNA targets. *Cell* **120**: 15–20.

Lewis BP, Shih IH, Jones-Rhoades MW, Bartel DP, Burge CB. (2003). Prediction of mammalian microRNA targets. *Cell* **115**: 787–798.

Menzel T, Rahman Z, Calleja E, White K, Wilson EL, Wieder R *et al*. (1996). Elevated intracellular level of basic fibroblast growth factor correlates with stage of chronic lymphocytic leukemia and is associated with resistance to fludarabine. *Blood* **87**: 1056–1063.

Mohammadi M, McMahon G, Sun L, Tang C, Hirth P, Yeh BK *et al*. (1997). Structures of the tyrosine kinase domain of fibroblast growth factor receptor in complex with inhibitors. *Science* **276**: 955–960.

Nakamoto T, Chang CS, Li AK, Chodak GW. (1992). Basic fibroblast growth factor in human prostate cancer cells. *Cancer Res* **52**: 571–577.

Navarro A, Diaz T, Gallardo E, Vinolas N, Marrades RM, Gel B *et al*. (2011). Prognostic implications of miR-16 expression levels in resected non-small-cell lung cancer. *J Surg Oncol* **103**: 411–415.

Polnaszek N, Kwabi-Addo B, Peterson LE, Ozen M, Greenberg NM, Ortega S *et al*. (2003). Fibroblast growth factor 2 promotes tumor progression in an autochthonous mouse model of prostate cancer. *Cancer Res* **63**: 5754–5760.

Polyak K, Weinberg RA. (2009). Transitions between epithelial and mesenchymal states: acquisition of malignant and stem cell traits. *Nat Rev Cancer* **9**: 265–273.

Risbridger GP, Taylor RA. (2008). Minireview: regulation of prostatic stem cells by stromal niche in health and disease. *Endocrinology* **149**: 4303–4306.

Roccaro AM, Sacco A, Thompson B, Leleu X, Azab AK, Azab F *et al*. (2009). MicroRNAs 15a and 16 regulate tumor proliferation in multiple myeloma. *Blood* **113**: 6669–6680.

Sahni A, Simpson-Haidaris PJ, Sahni SK, Vaday GG, Francis CW. (2008). Fibrinogen synthesized by cancer cells augments the proliferative effect of fibroblast growth factor-2 (FGF-2). *J Thromb Haemost* **6**: 176–183.

Sezer O, Jakob C, Eucker J, Niemoller K, Gatz F, Wernecke K *et al*. (2001). Serum levels of the angiogenic cytokines basic fibroblast growth factor (bFGF), vascular endothelial growth factor (VEGF) and hepatocyte growth factor (HGF) in multiple myeloma. *Eur J Haematol* **66**: 83–88.

Shin VY, Jin H, Ng EK, Cheng AS, Chong WW, Wong CY *et al*. (2011). NF-κB targets miR-16 and miR-21 in gastric cancer: involvement of prostaglandin E receptors. *Carcinogenesis* **32**: 240–245.

Smith JA, Madden T, Vijjeswarapu M, Newman RA. (2001). Inhibition of export of fibroblast growth factor-2 (FGF-2) from the prostate cancer cell lines PC3 and DU145 by Anvirzel and its cardiac glycoside component, oleandrin. *Biochem Pharmacol* **62**: 469–472.

Song S, Wientjes MG, Gan Y, Au JL. (2000). Fibroblast growth factors: an epigenetic mechanism of broad spectrum resistance to anticancer drugs. *Proc Natl Acad Sci USA* **97**: 8658–8663.

Thiery JP. (2002). Epithelial-mesenchymal transitions in tumour progression. *Nat Rev Cancer* **2**: 442–454.

Thiery JP, Acloque H, Huang RY, Nieto MA. (2009). Epithelial-mesenchymal transitions in development and disease. *Cell* **139**: 871–890.

Turner N, Pearson A, Sharpe R, Lambros M, Geyer F, Lopez-Garcia MA *et al*. (2010). FGFR1 amplification drives endocrine therapy resistance and is a therapeutic target in breast cancer. *Cancer Res* **70**: 2085–2094.

Tuxhorn JA, Ayala GE, Smith MJ, Smith VC, Dang TD, Rowley DR. (2002). Reactive stroma in human prostate cancer: induction of myofibroblast phenotype and extracellular matrix remodeling. *Clin Cancer Res* **8**: 2912–2923.

van Moorselaar RJ, Voest EE. (2002). Angiogenesis in prostate cancer: its role in disease progression and possible therapeutic approaches. *Mol Cell Endocrinol* **197**: 239–250.

Wernert N, Kaminski A, Haddouti el M, Hahne JC. (2007). Tumor-stroma interactions of metastatic prostate cancer cell lines: analyses using microarrays. *Methods Mol Biol* **382**: 223–237.

Winter SF, Acevedo VD, Gangula RD, Freeman KW, Spencer DM, Greenberg NM. (2007). Conditional activation of FGFR1 in the prostate epithelium induces angiogenesis with concomitant differential regulation of Ang-1 and Ang-2. *Oncogene* **26**: 4897–4907.

Wu HC, Hsieh JT, Gleave ME, Brown NM, Pathak S, Chung LW. (1994). Derivation of androgen-independent human LNCaP prostatic cancer cell sublines: role of bone stromal cells. *Int J Cancer* **57**: 406–412.

Yang F, Strand DW, Rowley DR. (2008). Fibroblast growth factor-2 mediates transforming growth factor-beta action in prostate cancer reactive stroma. *Oncogene* **27**: 450–459.

Zhang Y, Song S, Yang F, Au JL, Wientjes MG. (2001). Nontoxic doses of suramin enhance activity of doxorubicin in prostate tumors. *J Pharmacol Exp Ther* **299**: 426–433.

Supplementary Information accompanies the paper on the Oncogene website (http://www.nature.com/onc)